Reentrant ferroelectric phase induced by a tilting high magnetic field in $Ni_3V_2O_8$

C. Dong,[1] J. F. Wang,[1,*] Z. Z. He,[2] Y. T. Chang,[1] M. Y. Shi,[1] Y. R. Song,[1] S. M. Jin,[1] Y. Q. Du,[1] Z. Y. Wu,[1] X. T. Han,[1] K. Kindo,[3] and M. Yang[1,†]

[1]*Wuhan National High Magnetic Field Center and School of Physics, Huazhong University of Science and Technology, Wuhan 430074, China*

[2]*State Key Laboratory of Structural Chemistry, Fujian Institute of Research on the Structure of Matter, Chinese Academy of Sciences, Fuzhou, Fujian 350002, China*

[3]*The Institute for Solid State Physics (ISSP), University of Tokyo, Chiba 277-8581, Japan*

(Received 26 November 2021; accepted 19 January 2022; published 31 January 2022)

The canonical multiferroic material $Ni_3V_2O_8$ with a kagome staircase structure of $S = 1\,Ni^{2+}$ spins has attracted much attention for its complex magnetic phase diagram, as well as the interplay between spin orders and ferroelectricity. In the present work, we report a comprehensive angular dependent ferroelectric polarization study on $Ni_3V_2O_8$ with the field rotating within the *ac* plane at low temperatures. The low field induced ferroelectric (LF) state along the crystallographic *b* axis, which has been observed when the field is applied parallel to the easy axis (*a* axis), is revealed to vanish suddenly as the field is rotating close to the *c* axis. Of particular interest is the observation of the reentrant ferroelectric (HF) phase at high field for various orientations when the field is between the *a* and *c* axes within a small angle range. The field-angle phase diagrams are built based on the low-temperature angular dependent polarization results and composed of a continuous LF phase and a discontinuous HF phase both exhibiting symmetry with respect to the *a* axis. The microscopic origins of the two phases are different due to the two decoupled sublattices in the kagome staircase structure, where the low-field polarization is proposed to originate from the spiral structure of the spine spins, while the high-field phase is ascribed to the ordering of the cross-ties under a tilting high magnetic field.

DOI: 10.1103/PhysRevB.105.024427

I. INTRODUCTION

The essential geometric spin frustration in the kagome lattice has attracted tremendous research interest during the past decades, leading to exotic properties and candidature of the quantum spin liquid states [1,2]. Along with the inversion symmetry breaking induced by the geometric distortion, ferroelectric order has been realized in buckled kagome staircase lattice compounds [3–6]. The frustration of spins in the kagome staircase plays a central role by introducing noncollinear spin texture and thus multiferroics. The $M_3V_2O_8$ family—with *M* being the divalent cation, varying among Mn, Ni, Co, and Cu—is a representative kagome staircase structure [7,8]. Among the *M*VO family, $Ni_3V_2O_8$ (NVO) has become a canonical example of a multiferroic system which has drawn considerable interest due to its rich magnetic phase diagram, provided the magnetic and ferroelectric orders are strongly coupled [5]. Comparable interlayer interaction with intralayer interaction, as well as a high interlayer lattice constant, both reduce spin frustration through interlayer exchange coupling [9–12].

NVO crystalizes in orthorhombic space group *Cmca* with lattice constants $a = 5.931(6)$ Å, $b = 11.374(8)$ Å, and $c = 8.235(5)$ Å [13]. The abundant magnetic and novel multiferroic properties of NVO are determined by the magnetic $S = 1\,Ni^{2+}$ ions [9]. There are two distinct types of Ni^{2+} ions which are defined as "spine" and "cross-tie" sites, forming a buckled kagome staircase layer with edge-sharing NiO_6 octahedra in the *ac* plane. Figure 1(a) shows the kagome network of Ni^{2+} ions in NVO, with the two types of Ni^{2+} ions indicated in red (spine) and blue (cross-tie). The buckled staircase geometry distorted from the ideal kagome lattice has induced high anisotropy, leading to additional interactions compared to a conventional geometrical frustrated kagome lattice system. The significant competing next-nearest interaction produces noncollinear spin configurations with long-range modulation and contributes to additional ferroelectric and magnetoelectric (ME) properties. The interplay of a series of interactions such as the competition between the nearest and second-nearest interactions, anisotropic interactions, and pseudodipolar and Dzyaloshinskii-Moriya (DM) interactions plays a center role in yielding a rich and anisotropic phase diagram [5,9,14–16]. In the absence of magnetic field, NVO undergoes four different magnetic ordered phase transitions at low temperatures below ~9 K (the Néel temperature T_N), entering a high-temperature incommensurate phase (HTI), a low-temperature incommensurate phase (LTI), and two commensurate phases named as C and C′ as the temperature decreases. The spin order in the HTI state has been determined to focus on the spines with their spins parallel to the *a* axis, while in the LTI phase the spins of both spine and cross-tie sites rotate within the *ab* plane. This spiral spin configuration in the LTI phase gives rise to spontaneous electric polarization parallel to the crystalline *b* axis, according to the inverse Dzyaloshinskii-Moriya or the spin current

*jfwang@hust.edu.cn
†ming_yang@hust.edu.cn

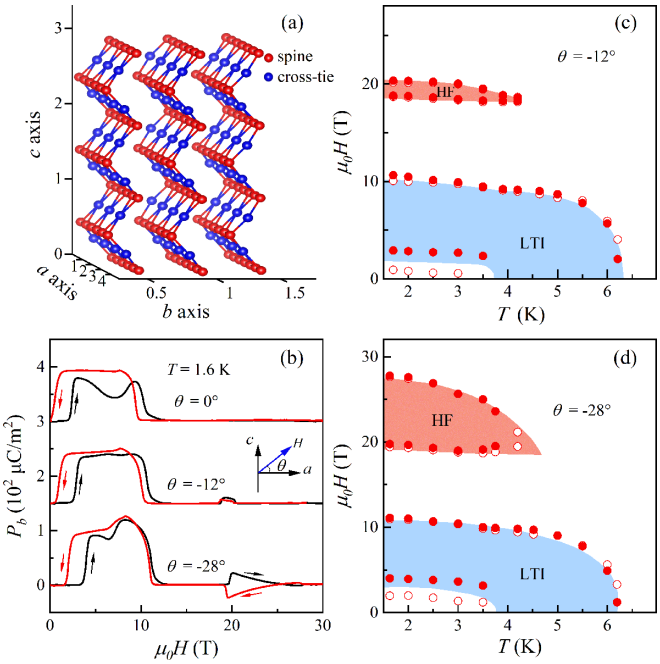

FIG. 1. (a) The crystal structure of NVO with a kagome staircase lattice, consisting of two different kinds of Ni^{2+} sites indicated as red (spines) and blue (cross-ties). (b) The electric polarization P_b as a function of H at $T = 1.6$ K under a bias electric field $\boldsymbol{E} = +500$ kV/m for three different field directions of $\theta = 0°$, $-12°$, and $-28°$, respectively. Black (red) lines represent the rising (falling) sweeps of the magnetic field pulses. (c), (d) The H-T phase diagram of P_b for two typical field directions of $\theta = -12°$ and $\theta = -28°$. The open (solid) symbols denote the decreasing (increasing) sweeps of the P-H curves.

mechanism: $P \propto e_{ij} \times (S_i \times S_j)$ [15,17]. The commensurate phase C at $T < 3.9$ K, described as a canted antiferromagnetic phase (CAF), is paraelectric due to the lack of broken inversion symmetry. However, the second paraelectric C′ phase was only detected by specific heat and thermal transport measurements [9,18]. The spin structure in the C′ phase has been revealed by elastic neutron scattering, which comprises the incommensurate ordering on the cross-tie and commensurate antiferromagnetic ordering on the spine sites [19]. The spins correspond to the cross-ties sites ordering into two cycloids with opposite helicities and the C′ phase is consequently also paraelectric as is the C phase.

Under the application of external magnetic field, the H-T phase diagram of NVO has been revealed to be complex, as a result of the competing magnetic interactions mentioned above. The sample shows a paraelectric (PE) to ferroelectric (FE) transition at a field range of 2–11 T at $T < 2$ K, indicating a field induced C to LTI phase transition. From the high-field studies on the magnetization and electric polarizations, a phase diagram revealing complex evolution of the phases and a unique high-field FE phase has been built [20,21].

The present paper focuses on the polarization P_b under tilting magnetic fields within the ac plane, to uncover the rich evolution with various spin structures for different magnetic field directions. We follow the same measurement strategy as Ref. [22], and build the H-θ phase diagrams at low temperatures. Our data reveal that the low-field (LF) phase is related with the spine spins, while the high-field (HF) phase, only appearing at a small range of field directions, originates from the ordering of the cross-tie spins under high fields. The H-θ phase diagrams elucidate that both the LF and HF phases are symmetrical with respect to the easy a axis and correlate closely with the spin structure in NVO. They also emphasize that the kagome staircase structure with both intralayer and interlayer competing interaction can provide a useful playground for the searching for field-induced ferroelectric polarization.

II. EXPERIMENT

High-quality single crystals of NVO were grown by the flux method with details reported in [23]. The crystal was carefully oriented by Laue x-ray photography. A thin plate sample of $2\times2\times0.2$ mm^3 was cut for the electric polarization measurements with the two largest surfaces normal to the crystallographic b axis. Two electrodes were attached to the two surfaces by silver paste. The pyroelectric current was measured by a 10 kΩ shunt resistor under a bias voltage of 100 V (which converts into a bias field of $\boldsymbol{E} = +500$ kV/m). The high-field polarization measurements were performed during a pulsed field of up to 30 T with a duration time of 10 ms in Wuhan National High Magnetic Field Center (WHMFC). Electric polarization was then obtained by integrating the pyroelectric current over the magnetic field H. Prior to the low-temperature P measurements, a poling field of typically 500 kV/m was also applied to form a single domain phase of the ferroelectric state during the cooling procedure. Angular dependent measurements were performed using a quartz dial plate [24,25].

III. RESULTS

We first measured the electric polarization along the crystallographic b axis measured in magnetic fields parallel to the a axis at low temperatures $T = 1.6$ K. Figure 1(b) presents P_b as a function of H applied along the a axis, as well as a tilting angle $\theta = -12°$ and $-28°$ within the ac plane. Note that θ is described as the angle between the field direction and the a axis within the ac plane with $\theta = +90°$ for the $+c$ and $-90°$ for $-c$. For $H \parallel a$, a field-induced polarization P_b of around 100 μC/m^2 emerges between $\mu_0 H_1 = 3.4$ T and $\mu_0 H_3 = 11$ T during the rising sweep of the magnetic field pulse, which can be attributed to the LTI phase confirmed by its temperature development (shown in the Supplemental Material [26]). The transition at H_3 is attributed to the LTI phase to a collinear spin configuration, where the unusual 1/2-magnetization plateau is established [20]. As the field sweeps back, hysteretic behavior at H_1 and H_3 can be discerned between the increasing and decreasing sweeps, indicating the first-order transitions at boundaries of the LTI phase. This observation of the only low-field (LF) FE phase at low-field range is in good agreement with a previous report by Wang *et al.* [20], but contradicts a later study by Liu *et al.* [21] where a high-field (HF) FE was detected under high field. In the present study, we find that the HF phase can only be

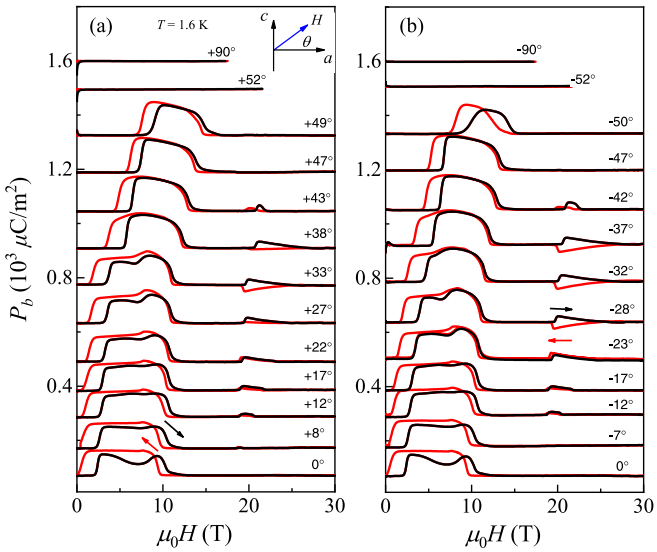

FIG. 2. The magnetic field dependence of P_b with field applied along different directions within the *ac* plane at $T = 1.6$ K. The inset shows the setup for the angular dependence measurements. The magnetic field H rotates within the *ac* plane and θ denotes the angle between the magnetic field and the *a* axis. Black (red) curves in the main panel denote the data obtained during the increasing (decreasing) sweep of magnetic field pulses.

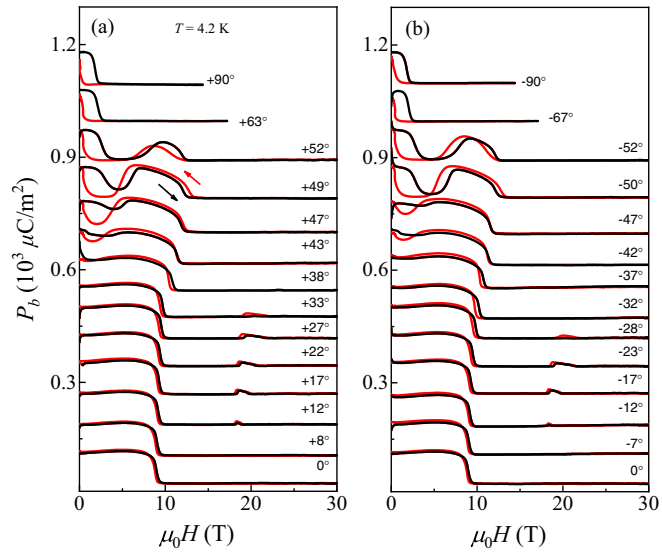

FIG. 3. The magnetic field dependence of P_b with field applied along different directions within the *ac* plane at $T = 4.2$ K.

observed when the magnetic field is tilted away from the *a* axis within the *ac* plane. As also shown in Fig. 1(b), the polarization P_b at $\theta = -12°$ and $-28°$ shows a HF phase under field between 19 and 26 T, along with the observed LF phase at between H_1 and H_3. The HF phase is also interesting for its polarization reversal behavior, where the sign of P_b in the increasing sweeps in one pulse is opposite to that in the decreasing sweeps.

Based on a temperature dependence study of P_b for $\theta = -12°$ and $-28°$ (see the Supplemental Material [26]), we have constructed the *H-T* phase diagram of NVO at these two particular angles. Figures 1(c) and 1(d) present the FE phase diagram for $\theta = -12°$ and $\theta = -28°$, respectively. It is revealed that the HF phase is quite sensitive to the field direction, based on the obvious change of the HF area from $\theta = -12°$ to $\theta = -28°$. However, the low-field FE phase, which connects continuously with the LTI phase at zero field, is insensitive to the change of the field direction. Since the ferroelectric order in NVO is strongly coupled with its magnetic structure, it provides an approach to uncover the spin configuration and study the frustration properties from the angular dependence of the polarization properties.

Comprehensive evolution of P_b under tilting fields has been measured by rotating the field within the *ac* plane. Figure 2 shows the systematic angular dependent P_b under tilting magnetic field at $T = 1.6$ K. The magnetic field was rotated away from the *a* axis by an angle θ within the *ac* plane, i.e., θ for $= 0°$ or $H \parallel a$ and $\theta = 90°$ $(-90°)$ for $H \parallel c$ $(-c)$, with a bias electric field $\boldsymbol{E} = +500$ kV/m applied during all the measurements. As the field is tilted from the *a* to the *c* axis, the LF phase shows continuous evolution with its two transitions shifting towards higher field until $|\theta| < 53°$. For $|\theta| \geqslant 53°$, the LF phase suddenly disappears without any sign, showing completely no field-induced FE phase up to 30 T as $H \parallel c$. The HF phase at around 20 T is observed within a limited field direction when the angle is between $8°$ $(-7°)$ and $47°$ $(-47°)$. Meanwhile, the angle dependence of the HF phase is also interesting. As $\theta \leqslant 27°$ (or $\theta \geqslant -23°$), the polarities of the P_b within the HF are the same during the increasing and decreasing sweeps in one pulse. However, the polarization direction of the HF during the decreasing sweep reverses as the field is a little more tilted, i.e., $\theta = 33°$ or $-28°$. Further rotating the field, the *P* reversal behavior disappears at $\theta = 43°(-42°)$.

The angular dependence of the *P-H* curves at elevated temperature $T = 4.2$ K is also studied and shown in Fig. 3. At 4.2 K, NVO enters the LTI phase and shows spontaneous polarization. This is consistent with the observation in Fig. 3 that the sample shows a finite P_b at zero field for all the directions from $\theta = 0°$ to $\theta = \pm 90°$. Similar to the data at $T = 1.6$ K, the HF phase is also observed at a small angle range, except for the *P* reversal behavior observed at lower temperature. Another impressive finding is that the LF phase at 4.2 K divides into two subphase for $|\theta| > 47°$ and the higher-field subphase totally disappears at $|\theta| > 52°$. We note that the LF also shows a subtle minimum at $\mu_0 H_2 \sim 8$ T for $H||a$ at $T = 1.6$ K. It is possible that the LF at 1.6 K also consists of two subphases divided by H_2 and the two subphases merge as the field is tilted away from the *a* axis. While at 4.2 K, the two subphases are merged for $H \parallel a$ but separate as the field is tilted away from the *a* axis.

Based on the data presented in Figs. 2 and 3, we summarize the *H-θ* phase diagram of NVO. Figures 4(a) and 4(b) display the *H-θ* phase diagram at $T = 1.6$ and 4.2 K, respectively. The boundary is extracted from the first derivative of the P_b curves (the pyroelectric current I_p vs H). Open (closed) circles denote the critical fields determined by the decreasing (increasing) sweeps of field. Note that the polarity of P_b is not reflected in the phase diagram. At $T = 1.6$ K, the

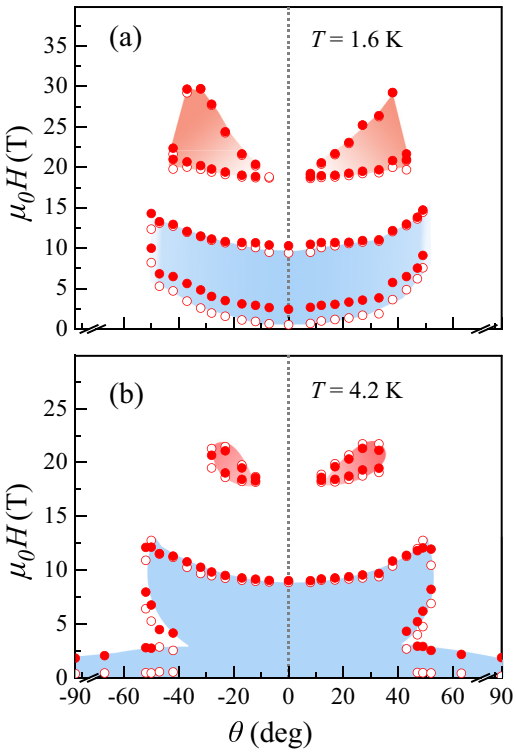

FIG. 4. The H-θ diagram determined from the angular dependence of the polarization data shown in Figs. 2 and 3. Open (closed) circles denote the critical fields determined by the decreasing (increasing) field sweeps.

presented phase diagram looks like a "happy pumpkin face" for Halloween, showing obvious symmetrical evolution with respect to the a axis ($\theta = 0^\circ$). Revealed by this phase diagram, the LF phase cuts off at a critical angle $\pm\theta_c$ ($\sim 52^\circ$). For the higher temperature of $T = 4.2$ K, shown in Fig. 3(b), the HF phase becomes smaller. However, the LF phase expands with its lower subphase occupying all the angles, while the higher subphase disappears at the same critical angles as for $T = 1.6$ K.

IV. DISCUSSION

Now, we discuss the implication of the present results in relation to the spin structure under various magnetic field directions. As mentioned above, the LF phase is intimately related to the LTI phase, where the spine spins rotate within the ab plane. At $T = 1.6$ K, NVO is within the C′ phase and the spine spins form a canted antiferromagnetic order along the a axis. For $\theta = 0^\circ$ shown in Fig. 2, i.e., $H \parallel a$, the magnetic field flops the spine spins and forms a cycloidal state of the spins rotating within the ab plane with its propagating vector running along the a axis, as in the LTI phase. The contribution of the cross-ties are negligible since the cross-tie spins remain disordered [27].This field-induced C to LTI phase transition is a result of the weak anisotropic interaction ($J_{\text{intra}}/J_{\text{inter}} \sim 2.6$) in NVO under a moderate field [5]. The theoretical explanation of this kind of field-induced transition in frustrated antiferromagnets has been discussed by Utesov and Syromyatnikov [28]. Since the spiral spin configuration of the spine spins would be wiped out along with the polarization of spins of the easy axis by high field, no electric polarization should emerge within the inversed DM scenario. It is consistent with the observation of the P_b curves along the $H \parallel a$ axis shown in Fig. 1(b), where only the LF phase is observed below H_3 and the disappearance of the FE state coincides well with the onset of the 1/2-magnetization plateau [20]. When the field is tilted, the two transition fields of the LF phase both shift to higher field. In some hexaferrite systems, the transition fields and the magnitude of the polarization both scale with the cosine relation, namely, the magnetically rotatable polarization effect which is dominated by the linear magnetoelectric (ME) effect [29,30]. In the case of NVO, however, the angular dependence of the transition fields does not fit with the cosine relation. The H-θ phase diagram at $T = 4.2$ K is somehow similar to its counterpart at $T = 1.6$ K, except for the clear splitting of LTI and the LF phase around the critical angle $\pm\theta_c$. It is clear that the LTI order at 4.2 K is suppressed by the magnetic field with a large component along the c axis (high angle for $|\theta| > \theta_c$) and a CAF order is built by H [5,31], whereas for $|\theta| < \theta_c$, the LF phase is connected continuously with the LTI phase, indicating a field enhanced stabilizing of the LTI phase. Therefore, it is reasonable to conclude that the magnetic field along the a axis can stabilize the LTI phase below H_3, while the field along the c axis suppresses the LTI rapidly. As proposed by Kenzelmann *et al.* [15], the Zeeman energy in an incommensurate phase under a field applied perpendicular to the staggered moments is larger than that of a field applied parallel due to the larger transverse susceptibility. Thus, it is energetically favored for a commensurate phase to form under a field along the c axis, which is manifested as a strong suppression on the LTI phase at 4.2 K and the vanishing of the field-induced LF phase for the $H \parallel c$ axis.

Meanwhile, the sudden cutoff of the LF phase at θ_c also raises questions. Both for $T = 1.6$ and 4.2 K, the phase diagrams have two different regimes: $|\theta| < \theta_c$ for the appearing of the field-induced LTI phase and $|\theta| > \theta_c$ for the disappearing. We now consider the ladder structure of NVO to explain this critical angle. Figure 5(a) shows the projection of the kagome staircase structure on the ac plane, within which the field is rotated. We notice that the direction of θ_c is very close to the direction pointed from a spine to its nearest neighbor cross-tie, ignoring the buckling of the kagome plane. Returning to the phase diagram for $T = 1.6$ K, we can summarize that a field applied along the direction running from a spine to its nearest cross-tie is a trigger for the disappearance of the field-induced LF phase. We suggest that the frustration on the cross-tie is strongly suppressed when the field is oriented at this critical angle. Revealed by the neutron elastic scattering results, the cross-tie spins are ordered in two counter-rotating cycloids within the bc plane with a period of five lattice constants along the c axis in the C′ phase [19]. Meanwhile, the easy axis of the cross-tie moments is reported to be the c axis due to the different ion anisotropy compared with the spines [32]. The external field destroys the spiral structure on the cross-ties and forms AF spin structure. The staggered moments on the cross-ties hence affect the four surrounding spines and suppress the cycloidal rotation of the spines within the ab plane and the LF

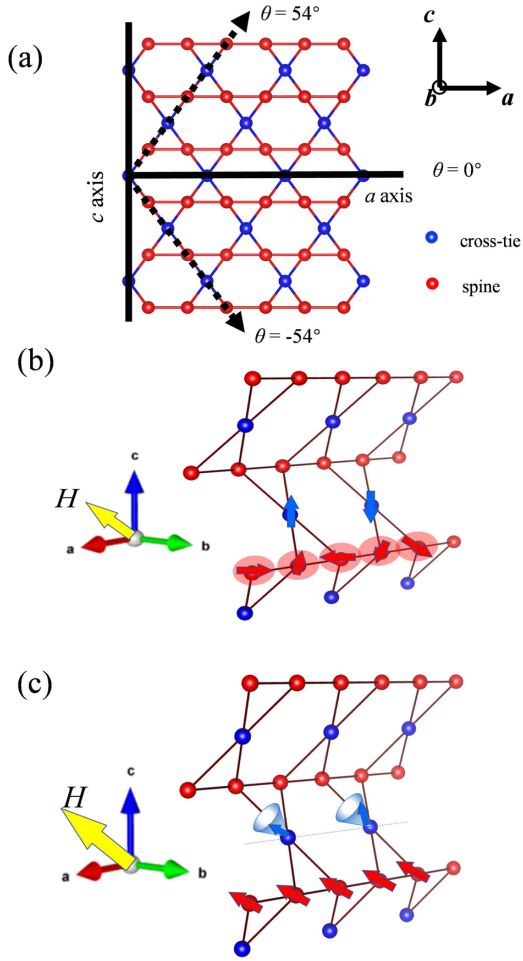

FIG. 5. (a) The side view along the *b* axis of the kagome staircase structure of the spine (red) and cross-tie (blue) sites. (b), (c) show the schematics of spin arrangements concerning the LF and HF under tilted field within the *ac* plane, respectively. The polarization in the LF phase arises from the cycloidal spiral structure on the spine moments, which is almost the same as in the LTI phase. At higher field, the HF phase under tilting fields originates from the formation of a canted conical structure of the cross-tie moments.

polarization phase is subsequently absent for the field close to the *c* axis.

Here we comment on the observation of the HF phases at a limited range of canted field direction. The emergence of the HF phase when the field is rotated away from the easy axis is rather interesting and deserves further investigation. In the case of NVO, we argue that the HF should be related to the cross-ties, since the spiral of the spins on the spines are already suppressed in the 1/2-magnezation plateau regime under high field. Compared to the CAF ordering of the spines in the C′ phase, the disordered state on the cross-tie indicates that the long-range interaction in the cross-tie net is weaker than that in the spines. Therefore, it requires a higher magnetic field to order the cross-tie spins to form a similar spin structure of the spines in the LF state. It is worth noting that the onset field (18 T) of the HF for $\theta = -12^\circ$ coincides well with a 2/3-magnetization step reported by Wang *et al.* [20], given that the magnetic moments on the cross-tie are half to that of the spines [32]. This correspondence confirms the association between the HF phase and the ordering of the cross-tie spins under high fields.

It can thus be suggested that a field-induced spiral spin structure correlated with the cross-ties is built under a tilting magnetic field [33]. Similar behavior has been reported in a hexaferrite $Ba_2Mg_2Fe_{12}O_{22}$, where the slanted magnetic field induces a transverse conical spin structure and tunes the polarization efficiently [34]. In Fig. 5(c), we propose a spin structure model of the cross-tie spins under a tilting high magnetic field. Since the HF is absent for the $H \parallel a$ axis, it is clear that the spiral structure is not as that in the LF phase, where the spine spins rotate in the *ab* plane to produce P_b [shown in Fig. 5(b)]. It is only possible that the cross-tie spins rotate in the *bc* plane with its propagating vector along the *a* axis. For $H \parallel a$, the cross-tie spins form a longitudinal conical structure, and thus $e_i \times e_j$ is parallel to e_{ij} (along the *a* axis) and no polarization can be produced. As the field is tilted, the spin cone axis is aligned to the external field and a canted conical structure is formed, which is responsible for the appearance of the HF phase. Further increasing the field, the spin cones are eventually closed by the alignment of the field, resulting in a linearly decreasing polarization within the field range of 18–24 T. Meanwhile, the spins on the spine should form a collinear structure which, manifested as a 1/2-magnetization plateau reported previously, produces zero polarization contribution in the high-field range. When the field is close to the critical angle, the higher field ($\mu_0 H > 20$ T) directly flops the cross-tie spins to the easy direction and prevents the formation of any spiral spin structures with broken inversion symmetry.

We finally discuss the polarization reversal behavior of the HF state during the increasing and decreasing sweeps of the field pulse. This sudden *P* reversal phenomenon upon the field sweeps resembles the memory effect that has been observed in $Co_2V_2O_7$ [35] and $MnWO_4$ [22,36,37]. In the case of $MnWO_4$, the reversal behavior emerges as the field is rotated close to the easy axis, when the vector spin chirality $C(= S_i \times S_j)$ of the conical spin structure is reversed by magnetic field. In $Ni_3V_2O_8$, the HF state exhibits two different scenarios: $|\theta| > 27^\circ$ for the presence of the *P* reversal and $|\theta| \leqslant 27^\circ$ for the absence of *P* reversal, where 27° is exactly half of θ_c. We argue that this coincidence is also related to the structure shown in Fig. 5(a). A possible reason can be the competition interaction between the spines and the cross-ties. Furthermore, the electric field control on the magnetic field dependent polarization also points out that this polarization reversal behavior between decreasing and increasing field is always present, irrespective to the polarity of the HF phase (see Supplemental Material [26]). It is reasonable to conclude that the chirality *C* of the canted conical structure is reserved and thus the polarity of P_b is retained during the increasing and decreasing sweeps for $|\theta| \leqslant 27^\circ$. On the other hand, when the field is applied for $|\theta| > 27^\circ$, the chirality *C* is reversed when the field sweeps back. The quantitative analysis of the chirality change for a high angle is beyond the scale of this work and deserves further investigation.

To summarize, we have performed a systematical study on the angular dependent polarization P_b of a kagome staircase

NVO under a magnetic field rotating within the *ac* plane. The H-θ phase diagrams have been constructed for $T = 1.6$ and 4.2 K. The H-θ phase diagrams reveal a LF phase and a HF phase, whose macroscopic origins are different due to the two decoupled sublattices in the kagome staircase structure. The LF is related to the spine spins whereas the discontinuous HF phase originates from the cross-tie spins. This work deepens the understanding of the spin structure and brings insights into field-induced ferroelectric polarization in frustration systems.

ACKNOWLEDGMENTS

We would like to thank C. L. Lu in the School of Physics, Huazhong University of Science and Technology for helpful discussions. This work was supported by the National Natural Science Foundation of China (Grants No. 12074135, No. U1832214, No. 51821005, No. 12004122, and No. 21875249) and the Fundamental Research Funds for the Central Universities (Grants No. 2018KFYXKJC005 and No. 2019KFYXJJS009).

[1] L. Balents, Nature (London) **464**, 199 (2010).
[2] S. Nishimoto, N. Shibata, and C. Hotta, Nat. Commun. **4**, 2287 (2013).
[3] K. Yoo, B. Koteswararao, J. Kang, A. Shahee, W. Nam, F. F. Balakirev, V. S. Zapf, N. Harrison, A. Guda, N. Ter-Oganessian, and K. H. Kim, npj Quantum Mater. **3**, 45 (2018).
[4] G. J. Nilsen, Y. Okamoto, H. Ishikawa, V. Simonet, C. V. Colin, A. Cano, L. C. Chapon, T. Hansen, H. Mutka, and Z. Hiroi, Phys. Rev. B **89**, 140412(R) (2014).
[5] G. Lawes, A. B. Harris, T. Kimura, N. Rogado, R. J. Cava, A. Aharony, O. Entin-Wohlman, T. Yildirim, M. Kenzelmann, C. Broholm, and A. P. Ramirez, Phys. Rev. Lett. **95**, 087205 (2005).
[6] S. N. Panja, L. Harnagea, J. Kumar, P. K. Mukharjee, R. Nath, A. K. Nigam, and S. Nair, Phys. Rev. B **98**, 024410 (2018).
[7] J. S. Helton, N. P. Butch, D. M. Pajerowski, S. N. Barilo, and J. W. Lynn, Sci. Adv. **6**, eaay9709 (2020).
[8] E. Morosan, J. Fleitman, T. Klimczuk, and R. J. Cava, Phys. Rev. B **76**, 144403 (2007).
[9] G. Lawes, M. Kenzelmann, N. Rogado, K. H. Kim, G. A. Jorge, R. J. Cava, A. Aharony, O. Entin-Wohlman, A. B. Harris, T. Yildirim, Q. Z. Huang, S. Park, C. Broholm, and A. P. Ramirez, Phys. Rev. Lett. **93**, 247201 (2004).
[10] Q. Zhang, W. Knafo, P. Adelmann, P. Schweiss, K. Grube, N. Qureshi, Th. Wolf, H. v. Löhneysen, and C. Meingast, Phys. Rev. B **84**, 184429 (2011).
[11] N. Qureshi, E. Ressouche, A. A. Mukhin, V. Yu. Ivanov, S. N. Barilo, S. V. Shiryaev, and V. Skumryev, Phys. Rev. B **88**, 174412 (2013).
[12] A. Kumarasiri and G. Lawes, Phys. Rev. B **84**, 064447 (2011).
[13] E. E. Sauerbrei, R. Faggiani, and C. Calvo, Acta Cryst. **29**, 2304 (1973).
[14] I. Cabrera, M. Kenzelmann, G. Lawes, Y. Chen, W. C. Chen, R. Erwin, T. R. Gentile, J. B. Leão, J. W. Lynn, N. Rogado, R. J. Cava, and C. Broholm, Phys. Rev. Lett. **103**, 087201 (2009).
[15] M. Kenzelmann, A. B. Harris, A. Aharony, O. Entin-Wohlman, T. Yildirim, Q. Huang, S. Park, G. Lawes, C. Broholm, N. Rogado, R. J. Cava, K. H. Kim, G. Jorge, and A. P. Ramirez, Phys. Rev. B **74**, 014429 (2006).
[16] R. C. Rai, J. Cao, S. Brown, J. L. Musfeldt, D. Kasinathan, D. J. Singh, G. Lawes, N. Rogado, R. J. Cava, and X. Wei, Phys. Rev. B **74**, 235101 (2006).
[17] I. A. Sergienko and E. Dagotto, Phys. Rev. B **73**, 094434 (2006).
[18] Z. Y. Zhao, Q. J. Li, X. G. Liu, X. Rao, H. L. Che, L. G. Chu, Z. Z. He, X. Zhao, and X. F. Sun, Phys. Rev. B **99**, 224428 (2019).
[19] G. Ehlers, A. A. Podlesnyak, S. E. Hahn, R. S. Fishman, O. Zaharko, M. Frontzek, M. Kenzelmann, A. V. Pushkarev, S. V. Shiryaev, and S. Barilo, Phys. Rev. B **87**, 214418 (2013).
[20] J. Wang, M. Tokunaga, Z. Z. He, J. I. Yamaura, A. Matsuo, and K. Kindo, Phys. Rev. B **84**, 220407(R) (2011).
[21] Y. J. Liu, J. F. Wang, Z. Z. He, C. L. Lu, Z. C. Xia, Z. W. Ouyang, C. B. Liu, R. Chen, A. Matsuo, Y. Kohama, K. Kindo, and M. Tokunaga, Phys. Rev. B **97**, 174429 (2018).
[22] J. F. Wang, W. X. Liu, Z. Z. He, C. B. Liu, M. Tokunaga, M. Li, C. Dong, X. T. Han, F. Herlach, C. L. Lu, Z. W. Ouyang, Z. C. Xia, K. Kindo, L. Li, and M. Yang, Phys. Rev. B **104**, 014415 (2021).
[23] Z. He, Y. Ueda, and M. Itoh, J. Cryst. Growth **297**, 1 (2006).
[24] Q.-Y. Liu, J.-F. Wang, H.-K. Zuo, M. Yang, and X.-T. Han, Acta Phys. Sin. **68**, 230701 (2019).
[25] W.-X. Liu, R. Chen, Y.-J. Liu, J.-F. Wang, X.-T. Han, and M. Yang, Acta. Phys. Sin. **69**, 057502 (2019).
[26] See Supplemental Material at http://link.aps.org/supplemental/10.1103/PhysRevB.105.024427 for the detailed temperature dependent measured for two typical field directions ($\theta = -12°$ and $-28°$) and the electric bias field control on the polarization reversal behavior for $\theta = 28°$.
[27] F. Fabrizi, H. C. Walker, L. Paolasini, F. de Bergevin, T. Fennell, N. Rogado, R. J. Cava, Th. Wolf, M. Kenzelmann, and D. F. McMorrow, Phys. Rev. B **82**, 024434 (2010).
[28] O. I. Utesov and A. V. Syromyatnikov, Phys. Rev. B **100**, 054439 (2019).
[29] K. Taniguchi, N. Abe, S. Ohtani, H. Umetsu, and T. Arima, Appl. Phys. Express **1**, 031301 (2008).
[30] T. Kimura, G. Lawes, and A. P. Ramirez, Phys. Rev. Lett. **94**, 137201 (2005).
[31] N. Qureshi, E. Ressouche, A. A. Mukhin, V. Yu. Ivanov, S. N. Barilo, S. V. Shiryaev, and V. Skumryev, Phys. Rev. B **94**, 174441 (2016).
[32] N. R. Wilson, O. A. Petrenko, and L. C. Chapon, Phys. Rev. B **75**, 094432 (2007).
[33] Y. Tokura, S. Seki, and N. Nagaosa, Rep. Prog. Phys. **77**, 076501 (2014).
[34] S. Ishiwata, Y. Taguchi, H. Murakawa, Y. Onose, and Y. Tokura, Science **319**, 1643 (2008).
[35] R. Chen, J. F. Wang, Z. W. Ouyang, Z. Z. He, S. M. Wang, L. Lin, J. M. Liu, C. L. Lu, Y. Liu, C. Dong, C. B. Liu, Z. C. Xia, A. Matsuo, Y. Kohama, and K. Kindo, Phys. Rev. B **98**, 184404 (2018).
[36] H. Mitamura, H. Nakamura, T. Kimura, T. Sakakibara, and K. Kindo, J. Phys.: Conf. Ser. **150**, 042126 (2009).
[37] K. Taniguchi, N. Abe, S. Ohtani, and T. Arima, Phys. Rev. Lett. **102**, 147201 (2009).